A Numerical Analysis of Stone Masonry Arch Bridges and Structural Backing

Thomas Kerr[1,2], Tomás O,Flaherty[1]
[1]Department of Civil Engineering and Construction, Institute of Technology Sligo, Ash Lane, Sligo, F91 YW50, Ireland
[2]National Roads Office, Drumlonagher, Donegal Town, F94 DK6C, Ireland.
email: thomas.kerr@mail.itsligo.ie, thomas.kerr@dnrdo.ie, oflaherty.tomas@itsligo.ie

ABSTRACT: Masonry arch bridges are a significant part of the transport network system in Ireland. Sustainability, economics and heritage point towards preservation. The increased demands placed on masonry bridges require a greater understanding of enhancing their structural features. Structural backing has been included in the construction of arches in the past to enhance the quality of arch construction. However, little is known of the contributions of structural backing to arch strength. The objective of this research is to determine what capacity enhancement can be gained by the presence of structural backing. Finite element analysis using ANSYS is used to generate 3D models of one segmental and one elliptical arch bridge in order to evaluate the effects of structural backing. The effects on arch capacity, stress distribution, deformation and failure mechanisms are investigated. Increased volumes of structural backing are found to have a significant influence on arch capacity. The model results indicate that a capacity increase of up to 25% for an elliptical arch and 27% for a segmental arch could be attained with concrete structural backing.

KEY WORDS: Masonry arch, structural backing, spandrel walls, finite element method

1 INTRODUCTION

The design of masonry arch bridges changed over time as better knowledge of perceived weaknesses in functional bridges led to improved design and construction practices. For example, higher quality material began to replace weaker fills in order to increase arch stability [1]. Bridges began to incorporate more enhanced features including internal spandrel walls in order to reduce weight and increase capacity by supporting arch thrust [2],[3]. Increased modern loading demands placed on our stone masonry arch bridges drive the exploration of how some of these higher quality features enable additional strength reserves. Such knowledge can also be used retrospectively in masonry arch strengthening programmes.

A number of approaches have been historically used in finite element (FE) modelling of arches. One-dimensional FE models were initially trialled [4], with a number of simplifying assumptions on fill and arch properties. Two-dimensional models can provide a better overall response and incorporate the use of more advanced constitutive masonry and soil models [5],[6],[7] but as the model is two-dimensional its response is based on simplifying planar assumptions. Three-dimensional (3D) modelling of masonry arches enables account to be taken of the full transverse behaviour of the bridge in response to loading and the effect of the outer spandrel walls. Macro-models, using continuum homogenous arch geometry and applying reduced material properties to account for the mortar interface in combination with a smeared crack formulation applied to the arch, have been used [8],[9]. Micro-models have also been used in a similar way but with interfaces between adjacent masonry units modelled [10].

1.1 Research Significance

The focus of this study was to use 3D FE models to evaluate how varying the extents of structural backing material could affect arch capacity. The research presented here adopts a micro-modelling approach with individual voussoir units modelled and separated by contact frictional interfaces to model the joints. Two existing masonry arch bridges were used to validate the accuracy of the 3D model and ultimately to test the effects, using a parametric study, that a hypothetical structural backing material has on the response of an arch when subject to loading.

2 METHODOLOGY

2.1 Existing Bridges

Two different bridges were used in this numerical study, as shown in Figures 1 and 2. The bridges modelled included a single span elliptical arch, denoted Bridge No.1, and a single span segmental circular arch, denoted Bridge No.2.

Figure 1: Elliptical arch Bridge No. 1 [9]

Figure 2: Segmental circular arch Bridge No. 2

Bridge No.1 has a span length of 9.49m, a rise at crown of 2.67m, an arch thickness of 0.45m and has an out-to-out width of 7.85m. The arch voussoir facing stones are of ashlar granite construction, while the internal arch barrel is of a limestone ashlar construction with joint widths of approximately 5mm. Bridge No.1 has been the subject of previous FE studies [8],[9] and valuable experimental load deflection data exists which was used in this study to validate the 3D FE model. Bridge No. 2 has a span length of 6.17m, a rise at crown of 1.81m, an arch thickness of 0.45m and has an out-to-out width of 8.10m. The arch facing voussoir is of a higher quality limestone square cut construction compared with that of the internal arch barrel, which is constructed using a more random rubble limestone with joint widths of between 10mm and 25mm.

2.2 Constitutive model for the backfill

The constitutive Mohr-Coulomb failure criterion is used to model the backfill is based on the Coulomb failure criterion, and is defined in terms of cohesion and angle of friction at a given level of stress, as shown in equation (1).

$$\tau = c - \sigma_n Tan\ \phi \qquad (1)$$

Stress invariants enable elemental orientation that is independent of the co-ordinate system. Equation (1), expressed in terms of these stress invariants, enables a plot of the function in principal stress space (Adpated from [11]):

$$F_S = \frac{I_1}{3} Sin\ \phi + \sqrt{J_2}\left[Cos\ \theta - \frac{1}{\sqrt{3}} Sin\ \theta\ Sin\ \phi\right] - cCos\ \phi \qquad (2)$$

Where, θ is the Lode angle, I_1 is the first invariant and J_2 is the second invariant of the deviatoric part arising from the decomposition of the Cauchy stress tensor.

The material, at failure, is assumed as isotropic. The failure surface is an irregular tapering hexagon, as shown in Figure 3. This shape arises from neglecting the effects of the intermediate principal stress. The tapering effect indicates that the material is pressure sensitive and enhanced shear strengths result from increasing principal stresses, represented by the increasing deviatoric plane along the hydrostatic axis, and of which a limiting value exists. A limiting tensile capacity can be established and is known as the tension cut-off. Cohesion, angle of friction and angle of dilation represent the plastic performance of the soil, and the Young's Modulus and the Poisson's ratio controls elastic responses.

2.3 Finite elements and meshing

The SOLID186 higher order 20-node element in ANSYS, with three degrees of freedom per node, was used to model both the masonry and fill. The reader is referred to the ANSYS software for further details of the element [13].

Frictional contact interfaces were used between adjacent masonry units. The coefficient of friction between adjacent masonry units was set at 0.7, with a value of 0.5 used between masonry and backfill, which is consistent with the literature [14]. The frictional formulation is based on the Augmented Lagrange, a penalty-based formulation where the contact stiffness influences the degree of penetration of both bodies [13]. The Augmented Lagrange formulation updates the stiffness value of the contact for increasing contact force. A stiffness factor of 1 was applied, given that the problem is broadly associated with bulk volume of stiffer forms of material. High contact stiffness values are applied where low levels of penetration are expected to occur, such as in masonry. The stiffness was set to update at each iteration meaning that any stiffness reduction, as a result of applied loading, is accounted for in subsequent iterations. The contact surfaces were set to adjust to touch; removing any gaps or inter surface penetration and associated potential error in the contact formulation. The CONTA174 8-node and associated TARGE170 8-node element are used to model contacts, enabling frictional effects and separation between adjacent surfaces. The reader is referred to the ANSYS software for further details of the elements [13].

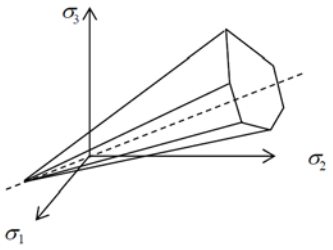

Figure 3: Mohr-Coulomb yield surface in principal stress space [12].

Figure 4 shows the hex-dominant mesh applied to the voussoir units, the spandrel walls, and structural backing. A tetrahedral mesh was applied to the backfill. A refined denser mesh was applied at the arch-fill interface and at points under loading, areas where stress concentrations were considered to be higher. Three elements were applied across the thickness of the arch and a mesh growth rate of 1.25 was applied.

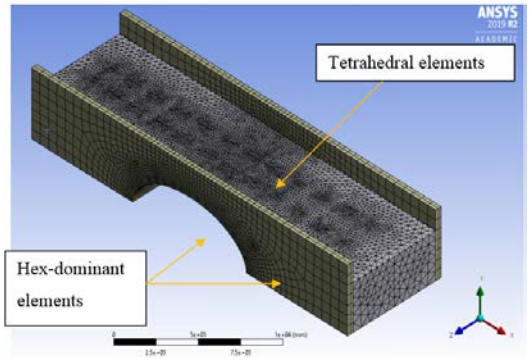

Figure 4: Example of a meshed model

2.4 Boundary conditions and loading

A displacement boundary condition was set at the base of the fill with no permissible movement in the X, Y and Z directions. The boundary conditions at the spandrel walls and abutments were defined by compression only supports. These boundary conditions were noted to permit small and not excessive horizontal deflections of the abutment into the fill. The ends of the model, including spandrel walls and the fill, were modelled as frictionless supports. The spandrel walls included in the model continued beyond their actual

dimensions where the fill spreads out into approach embankments. This assumption was valid as similar boundary conditions would be applied at these approach locations in order to retain the fill and the fill was not affected by arch loading at these remote locations. As loading and geometry were replicated either side of the centreline of the model, a symmetry plane was introduced to reduce the number of governing equations to be solved and hence computational expense.

2.5 Material Properties

Linear elastic material parameters were used to define the masonry and non-linear representation of the fill using the Mohr-Coulomb failure criterion, as summarised in Tables 1 and 2, respectively. For the fill material, the internal angle of friction and angle of dilation were taken as 44.43º, indicating that the Mohr-Coulomb model, at the plastic response, follows the associated flow rule.

Table 1: Masonry material properties for numerical models of Bridge No.1 and Bridge No.2

Poission's Ratio	Young's Modulus (Pa)	Density (kg/m^3)	Compressive Ultimate Strength (Pa)	Tensile Ultimate Strength (Pa)
0.3	$2.25x10^{10}$ (Bridge No.1) $1.25x10^{10}$ (Bridge No.2)	2200	$10\ x10^{6}$	$0.5\ x10^{6}$

Table 2: Backfill material properties used for constitutive models of Bridge No.1 and Bridge No. 2

Poission's Ratio	Young's Modulus (Pa)	Density (kg/m^3)	Cohesion (Pa)	Internal angle of friction (º)	Angle of dilation (Pa)
0.23	$0.5x10^{9}$	1700	3500	44.43	44.43

2.6 Analysis Settings

Large deflections were included to account for the non-linearity of the problem. Weak springs were added to overcome convergence issues and to tie contacting surfaces together, during initial loading substeps before stabilising compressive forces were generated. The solver used the Newton-Raphson force convergence to obtain solutions for each load step applied. Multi-step loading is applied at quarter points in each model case. The multi-step load is defined by a displacement boundary condition, as opposed to the direct application of force or pressure. The displacement boundary condition facilitates better convergence of the next displacement step even when the model cannot support additional force, such as during the formation of a hinge.

3 VALIDATION OF 3D MODEL

To ensure the 3D models were providing accurate approximations of masonry arch behaviour the results for the Bridge No.1 model were compared with experimental results [8]. The results obtained from the model provided good correlation with those obtained from the experimental findings, as can be seen in Figure 5. Deflection of the model was within 0.1mm of field measurements. It is noted that the FE model deflection curve is phased to the left of the experimental load test model, which could be attributable to, inter alia, the stiffer response generated by the FE model. As the model reflected the load-deflection behaviour of Bridge No.1, a parametric study to evaluate the effect of structural backing was undertaken. Validation of Bridge No.2 was not completed in the same manner as no experimental data was available. However, models for both bridges were developed using the same principles and similarly accurate behaviour would be expected for the model of Bridge No. 2.

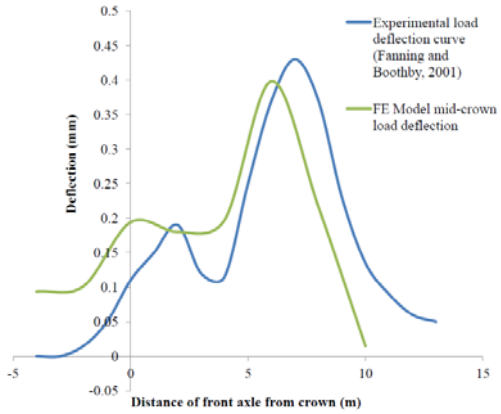

Figure 5: Comparison of experimental [8] and FE model deflections under moving vehicle load.

4 NUMERICAL PARAMETRIC STUDY

The primary objective of the research was to ascertain what effect structural backing has on arch capacity. Therefore, the parametric study focused on the relative behaviour of the two different arches with and without structural backing present over varying extents. The material properties of the concrete structural backing used in the models are given in Table 3. For the parametric studies, the concrete structural backing extents used in the models were brought to a quarter rise, half rise and three quarter rise and extended out by 500mm and 1000mm for each rise case. Figure 6 and Table 4 show details and dimensions of the structural backing for Bridge No.1 and No.2.

Table 3: Material properties for concrete structural backing

Poission's Ratio	Young's Modulus (Pa)	Density (kg/m^3)	Compressive Ultimate Strength (Pa)	Tensile Ultimate Strength (Pa)
0.18	$3x10^{10}$	2300	$4.1x10^{7}$	$0.5x10^{6}$

5 RESULTS AND DISCUSSION

5.1 Arch load-deflection behavior

The effects on load-deflection response caused by the addition of structural backing are shown in Figures 7 and 8. Generally, an increase in arch stiffness and capacity is observed with increasing volumes of structural backing material. The percentage increases in capacity with structural backing, compared with the model without backing, are highlighted in

Figures 9 and 10. With maximum structural backing extents, an increase in arch capacity of 25% and 27% occurs in Bridge No.1 and Bridge No.2, respectively.

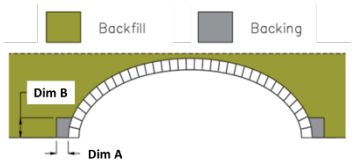

Figure 6: Location of concrete structural backing

Table 4: Dimensions of concrete structural backing

Bridge No. 1		Bridge No. 2	
Dim A (mm)	Dim B (mm)	Dim A (mm)	Dim B (mm)
500	790	500	565
1000	790	1000	565
500	1580	500	1130
1000	1580	1000	1130
500	2370	500	1695
1000	2370	1000	1695

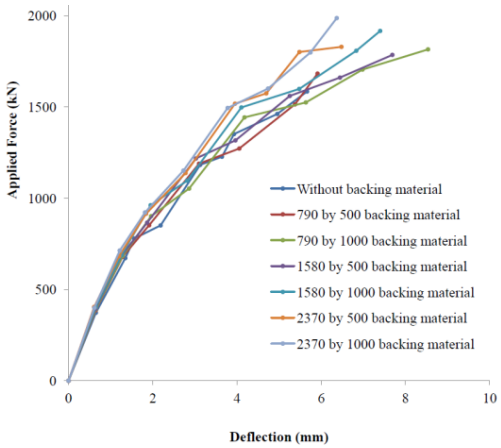

Figure 7: Load-deflection response for Bridge No. 1.

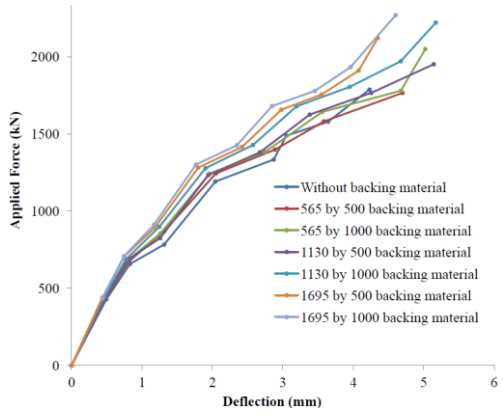

Figure 8: Load-deflection response for Bridge No. 2.

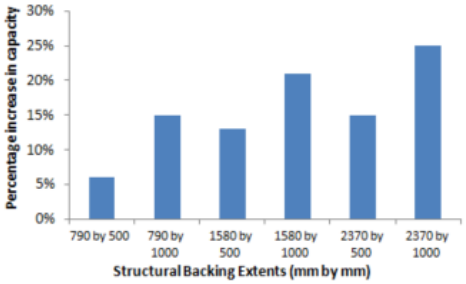

Figure 9: Percentage increase incapacity for Bridge No. 1.

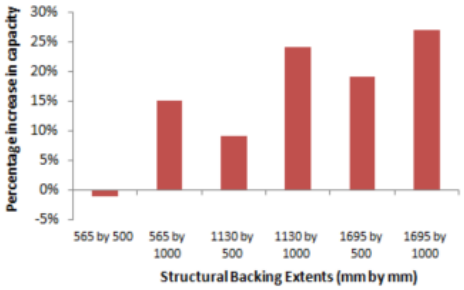

Figure 10: Percentage increase incapacity for Bridge No. 2.

The deformation behaviour of the arch before failure was similar for both bridges without and with backing, and is shown in Figures 11 and 12. The ultimate failure mechanism followed that of traditional arch failure theory, by the formation of a four-hinge mechanism [15]. In addition, transverse deflection is noted to be at a maximum directly under the loaded area and decreases towards the edges of the arch because of the stiffening effect of the external spandrel walls.

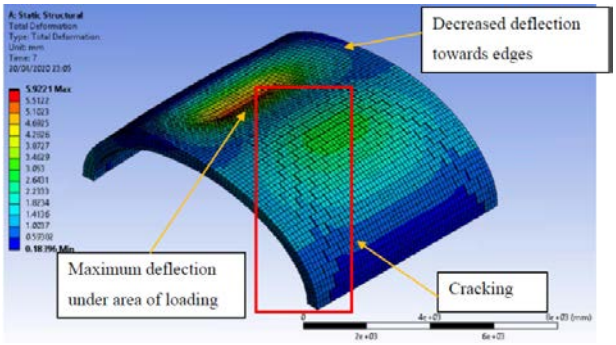

Figure 11: Deformation behaviour of Bridge No.1 without backing (only arch is shown for clarity).

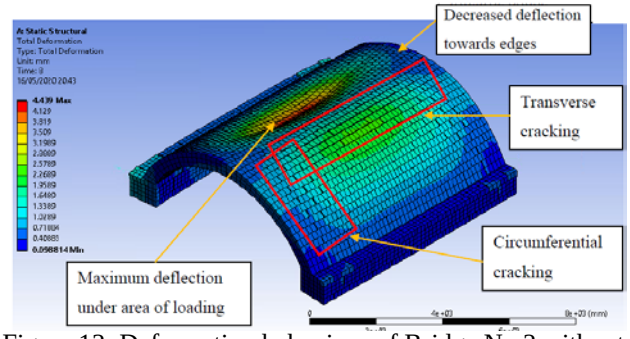

Figure 12: Deformation behaviour of Bridge No.2 without backing (only arch is shown for clarity).

In Bridge No. 1 diagonal cracking emanates from the areas of maximum deflection towards the edges, resulting in an 'X' type cracking formation, and indicating the three-dimensional response of the arch. In Bridge No. 2 transverse cracking occurs on the top side of the arch coinciding with the location of the third hinge. Circumferential cracking is noted towards the edges, where the deflecting arch is restrained by the spandrel wall. To understand this behaviour it is necessary to consider the process of hinge formation in the arches.

5.2 Hinge formation

All load-deflection curves presented in Figures 7 and 8 show intermittent changes in slope, transitioning from slope reduction to slope increase as load increased. This behaviour appeared to be coincident with hinge formation and subsequent stress redistribution within both arches, as shown for Bridge No. 1 in Figure 13

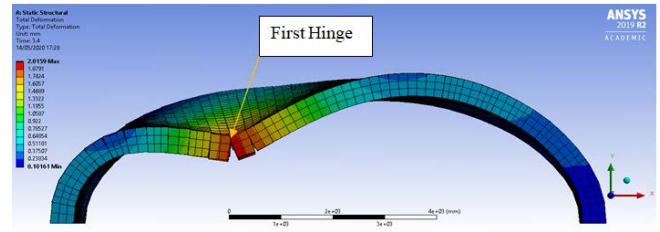

(a)

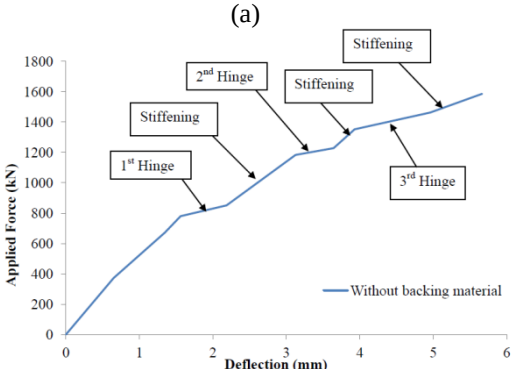

(b)

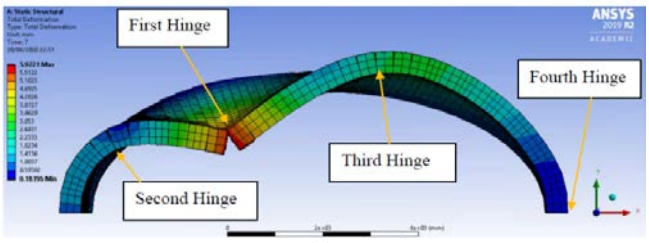

(c)

Figure 13: Model of Bridge No.1 without structural backing indicating (a) formation of first hinge, (b) load-deflection curve indicating hinge formation, and (c) location of all hinges.

Figure 13(a) shows the first hinge development at approximately 2mm deflection. The compressive stress on the arch extrados is approximately 4MPa, creating tension at the intrados and consequential hinge formation. This development corresponds with a reduction in the slope of the load-deflection curve in Figure13(b). The hinge forms about the arch extrados where the compressive stress is greatest and opening of a crack is observed on the non-tensile resistant intrados. The first hinge develops directly under the point of loading at a corresponding load of approximately 825kN. As the first hinge continues to form, the application of further loading causes the arch to stiffen as stress is redistributed. Compressive stress increases on the intrados to the left of the first hinge. In Figure 13(b) this is noted as a corresponding increase in the slope of the curve. The first hinge continues to open with increasing load. The formation of the second to fourth hinges follows the same process until failure of the arch at the formation of the fourth hinge, as show in Figure 13(c).

The presence of structural backing in the elliptical arch of Bridge No.1 alters the location and the sequencing of the fourth hinge formation. It moves from the base of the arch, Figure13(c), upwards to the point where the top of the structural backing meets the arch, as shown in Figure 14(a). The fourth hinge forms as the arch thrusts forward and is pushed into the structural backing on the unloaded side of the arch. This creates a localized compressive stress on the extrados. The exact location of the fourth hinge varied as the volume of structural backing material varied, but was observed to form at the joint in closest proximity to the top of where the structural backing met the arch. However, for the segmental arch of Bridge No. 2 a change in location of the fourth hinge did not occur, Figure 14(b), and the fourth hinge remained at the base of the arch. This behaviour is associated with the difference in thrust types between the two differing arch geometries of Bridge No.1 and No.2.

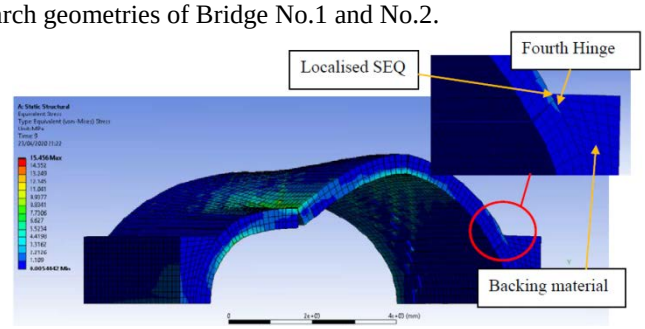

(a)

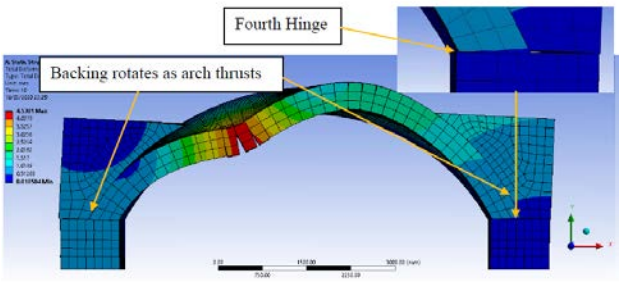

(b)

Figure 14: Location of fourth hinge in models with structural backing for (a) Bridge No.1, and (b) Bridge No.2

5.3 Stress distribution in arch

From Figures 7 and 8, it is clear that as the volume of structural backing increases, there is a corresponding increase in capacity for both bridges, and as a result, there is an associated increase in von-Mises stress (SEQ) within the backing material. The greater level of deflection in these models appears attributable to the degree of restraint provided by the backing material, with the lower volumes of backing

permitting greater arch deflection. The SEQ distribution in models for both bridges indicates that compressive stresses are generated within the backing material, as shown in Figure 15. This stress was found to increase with increasing load on the arch. During the formation of the first two hinges, the backing material to the left-hand-side supports the majority of this stress. As the third and fourth hinges form, and as the arch thrusts forward, the backing to the right-hand-side of the arch supports greater levels of stress.

A decrease in the compressive stress is experienced in the arch above abutment level where structural backing is present. A proportion of the stress is noted to disperse within the body of the backing material. With increasing backing material extents there is a corresponding decrease in the level of stress in the arch, as shown in Figure 16, for the indicated backing extents in Bridge No.1, by way of example.

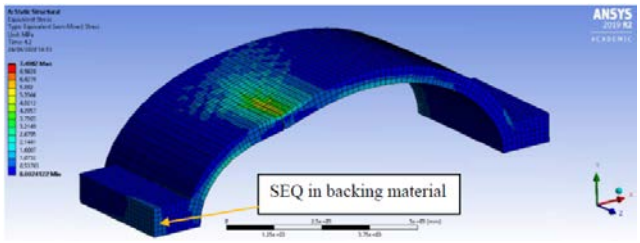

(a)

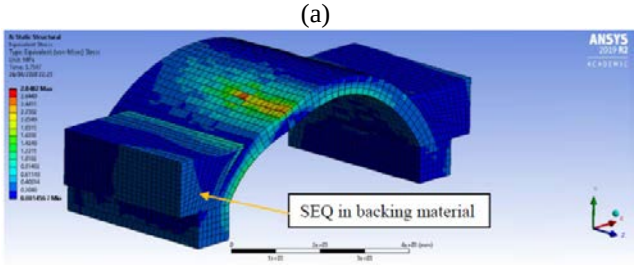

(b)

Figure 15: Distribution of SEQ in models with structural backing for (a) 790mm by 1000mm backing in Bridge No.1, and (b) 1130mm by 1000mm backing in Bridge No.2

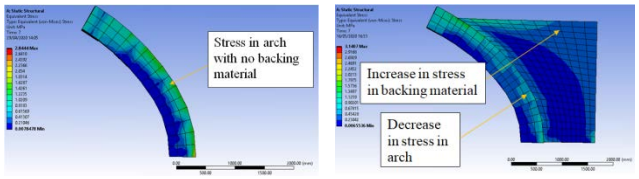

(a) (b)

Figure 16: von-Mises stress distribution in arch of Bridge No. 1 in (a) without backing material, and (b) with 2370mm by 1000mm backing material.

As the arch in Bridge No.1 is loaded on one side it thrusts forward into the backing material on the opposite side. Small compressive stresses are generated in the region where the arch is in contact with the backing material and this is the location where the fourth hinge ultimately forms. As this process causes the fourth hinge to move, the length of the arch is effectively shortened giving the arch decreased capacity to deflect under load. The backing provides a restraining effect enabling greater levels of compressive stress to be generated within the main body of the arch. A proportion of this compressive stress is dispersed within the structural backing material, when present. It is clear that a greater proportion of stress is dispersed into the backing material in models where a greater volume of backing material is present. Therefore, greater volumes of backing material have a greater influence on increasing arch capacity.

6 CONCLUSIONS

This paper presents findings from 3D FE models developed to evaluate the effects of structural backing material on masonry arch behaviour and capacity. The following conclusions are drawn from the results:

- It is possible to model the effects of structural backing using 3D discrete FE models for masonry arch bridges
- The models indicate that increasing volumes of backing, results in increasing capacity for elliptical and segmental circular arch models.
- The level of stress within the backing increases with increasing volumes of backing material.
- The results indicate that a capacity increase of 25% for the elliptical arch and 27% for the segmental arch is attained when concrete structural backing is brought to 1m beyond the arch and to 75% of the height of the rise of the arch.
- The presence of backing results in the alteration of the location and sequencing of hinge formation in an elliptical arch

ACKNOWLEDGMENTS

The research was possible by the making available of pertinent information by TII and support from DTTaS and DCC. The authors acknowledge the DJEI/DES/SFI/HEA Irish Centre for High-End Computing (ICHEC) for the provision of computational facilities and support.

REFERENCES

[1] Hosking, W. (1843). The Theory, Practice and Architecture of Bridges of Stone, Iron Timber and Wire. London: W. Hughes King's College London.
[2] Rankine, W. (1862). *A Manual of Civil Engineering.* London: Griffin, Bohn and Company.
[3] Telford, T. (1838). *Life of Thomas Telford.* London.
[4] Crisfield, M. (1985). Finite element and mechanism methods for the analysis of masonry and brickwork arches. Crowthorne: TRRL.
[5] Betti, A., Drosopoulos, G., & Stavroulakis, G. (2007). *On the collapse analysis of single span masonry/stone arch bridges with fill interaction* .
[6] Boothby, T. (1998). Service Load Response of Masonry Arch Bridges.
[7] Drosopolus, G., & Stavroulakis, G. (2006). Limit analysis of a single span masonry bridge with unilateral friction.
[8] Fanning, P., & Boothby, T. (2001). Three-dimensional modelling and full scale testing of stone arch bridges.
[9] Gibbons, N., & Fanning, P. (2016). Progressive cracking of masonry arch bridges.
[10] Pulatsu, B., Erdogmus, E., & Laurenco, P. (2018). Simulation of masonry arch bridges using discrete element modelling.
[11] Potts, D., & Zdravkovic, L. (1999). *Finite Element Analysis in Geotechnical Engineering.* London: Thomas Telford Publishing.
[12] Kelly, P. (2015). Solid Mechanics Part II - Engineering Solid Mechanics. Auckland.
[13] ANSYS. (2020). https://ansyshelp.ansys.com/account/secured?returnurl=/Views/Secured/corp/v201/en/ans_thry/thy_el174.html. Retrieved 01 10, 2020
[14] Dvorak, J., & Novak, L. (1994). *Soil Conservation and Silviculture.* Czeck Republic: Elsevier.
[15] Heyman, J. (1995). *The Stone Skeleton.* Cambridge: Cambridge University Press.